ACS APPLIED MATERIALS & INTERFACES

Research Article

www.acsami.org

Root-Cause Failure Analysis of Photocurrent Loss in Polythiophene:Fullerene-Based Inverted Solar Cells

Eszter Voroshazi,*[,†] Griet Uytterhoeven,[†] Kjell Cnops,[†,‡] Thierry Conard,[†] Paola Favia,[†] Hugo Bender,[†] Robert Muller,[†] and David Cheyns[†]

[†]imec, Kapeldreef 75, 3000 Leuven, Belgium

[‡]ESAT, Katholieke Universiteit Leuven, Kasteelpark Arenberg 10, 3001 Leuven, Belgium

Supporting Information

ABSTRACT: Metal oxide transport layers have played a crucial role in recent progress in organic photovoltaic (OPV) device stability. Here, we measure the stability of inverted and encapsulated polythiophene:fullerene cells with MoO_3/Ag/Al composite anode in operational conditions combining solar radiation and 65 °C. Performance loss of over 50% in the first 100 h of the aging is dominated by a drop in the short-circuit current (J_{sc}). We reveal a concurrent loss in reflectance from 85% to 50% above 650 nm, which is below the optical gap of the used photoactive materials, hence, excluding any major degradation in the bulk of this layer. Correlating the responses of aged devices to a series of test structures comprised of ITO/ZnO cathode, MoO_3/Ag, and MoO_3/Ag/Al anodes and their combinations with the active layer allowed us to identify that the presence of Al causes the reduced reflectance in these devices, independent of the presence of the active layer. Systematic single-stress aging on the test structures further indicates that elevated heat is the cause of the reflectance loss. Cross-section transmission electron microscopy coupled with elemental analysis revealed the unsuspected role of Al; notably, it diffuses through the entire 150 nm thick Ag layer and accumulates at the MoO_3/Ag interface. Moreover, XRD analysis of the aged MoO_3/Ag/Al anode indicates the formation of Ag_2Al alloy. Depth profiling with X-ray photoelectron spectroscopy advanced our understanding by confirming the formation of Ag−Al intermetallic alloy and the presence of oxidized Al only at the MoO_3/Ag interface suggesting a concomitant reduction of MoO_3 to most probably MoO_2. This latter compound is less reflective than MoO_3, which can explain the reduced reflectance in aged devices as proven by optical simulations. On the basis of these results, we could estimate that 20% of the loss in J_{sc} is ascribed to reduction of MoO_3 triggered by its direct contact with Al.

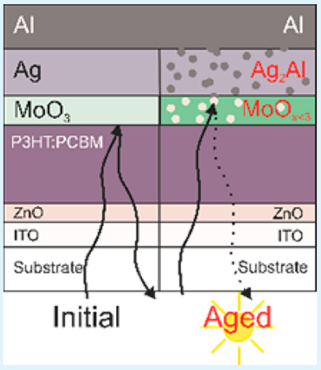

KEYWORDS: *organic photovoltaics, molybdenum oxide, degradation, diffusion, TEM, XPS*

1. INTRODUCTION

Performance of organic photovoltaic cells (OPVs) has rapidly leaped beyond the threshold of 10% power conversion efficiency in laboratory scale devices.[1] Simultaneous progress in device stability and large-area deposition is crucial to the prompt market introduction of OPVs. Accelerated evaluation of outdoor operational stability is usually conducted by measuring devices under continuous illumination, optionally combined with elevated temperature. In these conditions stable outdoor (extrapolated) device lifetime of 3−7 years has been reported, depending on the device architecture and packaging technology. It is important to note that extrapolation in these studies is based on the equivalence in light dose between the accelerated (laboratory) and outdoor exposure.[2,3] This stability already matches the requirements of mobile energy harvesting applications; however, the benefits of further enhanced device stability are manifold. As the levelized cost of energy (LCOE) strongly depends on the degradation rate, further improvements can enhance the competitive advantage of OPVs among PV technologies. Furthermore, reduced degradation rate would also enable the penetration of OPVs in building and/or vehicle-integrated applications where requirements are more stringent. This progress requires stability-conscious device and material design, which must be assisted by understanding the root causes of the performance loss. Our in-depth study aims to link the performance loss to optical and electrical changes of the transport layers, notably the changes in MoO_3, and elucidate mitigation strategies by revealing the underlying chemical degradation process(es). Stability of the electrodes and transport layers appear to be one of the most critical factors in the durability of devices. Replacement of the reactive low workfunction metal electrode by combination of nonreactive metals with metal oxides such as TiO_2 and ZnO was a critical milestone in the stability of OPVs, leading to multiple fold improvement in stability.[4−7] These oxide layers are often directly deposited on the glass coated with indium tin oxide (ITO), making the ITO the electron-collecting electrode, while the top contact with a high workfunction its hole-collecting

Received: October 2, 2014
Accepted: December 12, 2014
Published: December 24, 2014

DOI: 10.1021/am506771e
ACS Appl. Mater. Interfaces 2015, 7, 618−623

equivalent. Device polarity is inversed in this configuration compared to so-called conventional architecture cells. Similarly, MoO_3, V_2O_5, or WO_3 lead to superior stability relative to the commonly applied poly(3,4-ethylenedioxythiophene) polystyrenesulfonate (PEDOT:PSS) layer both in inverted and conventional architectures.[8,9] For these reasons, the currently most stable OPVs employ metal oxide layers on both sides of the photoactive layer. The overall device stability can be further strengthened by increasing the top metal thickness beyond 100 nm.[10] This is explained by the fact that penetration of oxygen and humidity in the device occurs along the metal/transport layer interface as well as through the defects in the metal layer. This latter process can be successfully mediated by using an over 100 nm thick Ag top contact; a more economical solution is a bilayer of Ag and Al. In inverted poly(3-hexylthiophene-2,5-diyl):phenyl-C61-butyric acid methyl ester (P3HT:PCBM) devices we have proven that the bilayer electrode increases device stability in air (without any encapsulation) by 1000 h compared to similarly thick Ag contacts.[11] Despite reaching similar initial performance on P3HT:PCBM cells with MoO_3/Ag and MoO_3/Al contacts, the latter configuration degrades considerably faster upon air exposure due to the formation of an insulating Al_2O_3 layer, which blocks charge extraction from the device. These arguments motivate our selection of MoO_3/Ag/Al as an air-stable and potentially light- and heat-stable contact layer. To assess the operational stability of this electrode, we selected to age prototypical P3HT:PCBM cells with inverted architecture, where the well-characterized degradation of these organic compounds enables discrimination between photoactive layer and electrode failure.[12−17] Accelerated aging conditions selected in our work match the extremes encountered in outdoor conditions such as 1 sun intensity, 65 °C ambient temperature, and 45% relative humidity (RH).[18] Continuous exposure to these elevated stress levels, following International Summit on OPV Stability (ISOS) protocols, enables the acceleration of the degradation mechanisms by removing day−night cycles.[18]

In the first part of the article, we describe the device performance decrease over 1000 h, which mostly arises from the loss of the photocurrent. Reflectivity measurement allows us to reveal that loss of this latter parameter is partially due to change in the optical parameters of the reflective top contact. Second, the systematic aging of numerous test structures in various aging conditions indicates the stress factor that triggers the failure. In the third part we further deepen our insights into the failure mechanism by corroborating the findings of transmission electron microscopy (TEM) analysis with energy-dispersive spectrometry (EDS), X-ray photoelectron spectroscopy (XPS), and X-ray diffraction (XRD). Finally we estimate the quantitative contribution of this failure process to the photocurrent loss by optical simulation relying on input from these material characterization techniques.

2. MATERIALS AND METHODS

2.1. Device Preparation. First, P3HT (Rieke Metals 4002EE) and $PC_{60}BM$ (Solenne bv.) in a 1:1 weight ratio were dissolved in a 2.5 wt % concentration in *ortho*-dichlorobenzene. Layers were deposited on previously cleaned and patterned ITO substrates. After the spin-coating of ZnO,[19] the active layer was deposited at 1000 rpm for 60 s to produce an ∼160 nm thick photoactive layer. Prior to metallization, the P3HT:$PC_{60}BM$ layers were annealed at 130 °C for 10 min in inert nitrogen environment. Samples were transferred to a metal evaporation chamber (base pressure 1×10^{-7} Torr) where 10 nm of MoO_3 (Aldrich) was deposited. Finally, 150 nm of Ag and 150 nm of Al are evaporated through a shadow mask defining 12 0.13 cm^2 area cells on a substrate. Samples are afterward sealed by attaching a second glass plate with UV-curable epoxy. Additionally, a humidity getter purchased from SAES was fixed inside the cavity glass.

2.2. Electrical Device Characterization and Aging. The initial and final photovoltaic characteristics were measured with a Keithley 2602 in two-wire configuration under a Lot Oriel Xenon arc lamp with 100 mW/cm^2 intensity and AM1.5D spectrum, calibrated with an ISE Fraunhofer certified Si photodiode. For external quantum efficiency (EQE) measurement a commercial setup (Bentham) was used. The light from Xe (300−670 nm) and quartz halogen lamps (670−900 nm) was coupled into a monochromator, and their intensities were calibrated with a Si photodiode. The incident light beam of a 0.7 mm diameter was chopped, and the modulated current signal was detected with a current−voltage and lock-in amplifier. The same optics and measurement setup was used with a DTR6 integrating sphere for reflectance measurement.

After the initial characterization, the samples were continuously illuminated in an ATLAS Suntest XXL system using xenon lamps with AM1.5G spectrum (and 60 W/m^2 dose of UV light between 300 and 400 nm) and 1 sun intensity. The chamber temperature and humidity were controlled during aging and fixed at 65 °C and 45% RH. The temperature of the samples during the illumination was approximately 85 °C as measured at the backside of the substrate. Samples were removed at regular intervals for electrical characterization at 25 °C. The samples were left in open-circuit between measurements. These aging conditions correspond to the ISOS-L2 protocol.[18] To decouple the effect of temperature and light, aging of test structures was conducted either on a hot plate at 85 °C (dark) or under solar light exposure in inert nitrogen atmosphere in a setup described earlier with a constant temperature of ∼35 °C.[13]

Optical simulation using the transfer matrix methodology formalism has been published earlier and relies on optical constant measured with ellipsometry (Sopralab, ges5 VASE).[20]

2.3. Chemical and Structural Characterization. Cross-section TEM specimens are prepared by focused ion beam (FIB) in a Strata 400S (30 kV Ga) by the lift-out method. A Tecnai F30 transmission electron microscope is used to investigate the specimen cross sections. This microscope is operated at 200 kV for acquiring images. Standard TEM and high-resolution (HR) TEM images are acquired by using a Gatan CCD camera, and HAADF-STEM and DF-STEM images are acquired with a Fischione detector. EDS is performed using an EDAX detector. The XPS measurements were carried out in Angle Integrated mode using a Theta300 system from Thermo Instruments. Sputter steps of 100 s were applied in between the measurements (80 levels). The measurements were performed using a monochromatized Al Kα X-ray source (1486.6 eV) and a spot size of 400 μm. X-ray reflectivity measurements were conducted on a PANalytical XPert Pro Materials Research Diffractometer using Cu Kα radiation.

3. RESULTS AND DISCUSSION

3.1. Description of Device Failure and Characterization of Device Packaging. Inverted architecture and sealed organic solar cells with the following layer stack: ITO/ZnO/P3HT:PCBM/MoO_3/Ag/Al were aged under continuous solar illumination. The chamber temperature was 65 °C, and temperature at the back side of the sample was ∼85 °C. (In the remainder of the article if devices are referred to as aged it refers to these conditions.) Electrical device parameters were measured at regular intervals and normalized to their initial value as shown in Figure 1. Device performance over 1000 h decreased by 50% compared to initial performance following a two-stage failure process dominated by the decline of the short-circuit current (J_{SC}, Table 1). The fast performance loss in the first 100 h of illumination, also called burn-in, followed an exponential decline, after which the current nearly entirely stabilizes. In the meantime, the open-circuit voltage (V_{OC}) and fill factor (FF) decrease by 20% and 10%, respectively, upon

DOI: 10.1021/am506771e
ACS Appl. Mater. Interfaces 2015, 7, 618−623

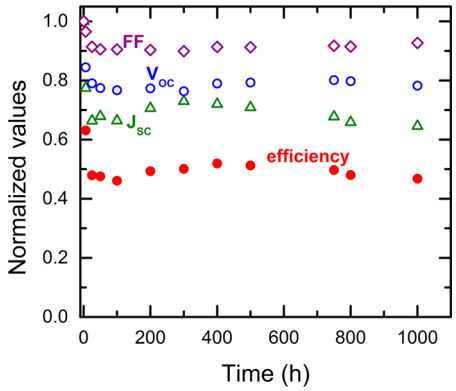

Figure 1. Evolution of normalized device performance parameters of glass-encapsulated ITO/ZnO/P3HT:PCBM/MoO_3/Ag/Al cells under 1 sun intensity and AM1.5G spectrum illumination. Sample temperature is kept at 85 °C, and the atmosphere humidity is 45% RH. Values are averages of 8−12 cells on a substrate.

Table 1. Average Device Parameters and Standard Deviation of ITO/ZnO/P3HT:PCBM/MoO_3/Ag/Al Cells before and after the 1000 h of Aging under Continuous Illumination

time, h	V_{OC} (mV)	J_{SC} (mA/cm^2)	FF (%)	PCE (%)
0	610.9 ± 2.4	10.2 ± 0.3	64.8 ± 1.5	4.03 ± 0.2
1000	566.3 ± 9.6	6.58 ± 0.3	50.7 ± 2.1	1.89 ± 0.1

100 h of illumination, while the J_{SC} declines by more than 30% during the burn-in stage.

Air ingress through the epoxy sealant could be one of the potential origins of the photocurrent loss. To quantify the air ingress we encapsulated 100 nm thick Ca samples with an identical process as that of the solar cells. Following the alteration in transparency of the Ca layer (cf. Supporting Information, Figure S2) allowed us to estimate the water vapor transmission rate (WVTR) and lag time of our packaging.[21,22] The onset of the Ca oxidation indicates that a steady ingress of air though the epoxy, that is, lag time, is established after approximately 50 h. As the entire Ca layer is oxidized upon 500 h of exposure we can estimate that the WVTR reaches 7 g/m^2/d at chamber temperature of 65 °C (and sample temperature close to 85 °C). Rapid performance loss already during the lag time of the package implies that contribution of air ingress to the failure is negligible during the burn-in, which is investigated in this study. Moreover, inverted cells are proven to be resilient to air exposure even in the presence of solar illuminations owing to their stable electrodes and transport layers.[10] Additionally the thick metal contact provides an additional encapsulation protecting the photoactive layer (not accounted for in our WVTR calculation).[23] Although ingress of oxygen and humidity can trigger the photooxidation in the photoactive layer, unchanged reflectance upon aging (Figure 2) below 650 nm, where the P3HT:PCBM blend absorbs, allowed us to exclude photobleaching as dominating failure mechanism. Unlike in the photoactive layer, reflectance of the transport and electrode layers above 650 nm is reduced from 85% to below 50%. This increase in parasitic absorption most probably extends over the full wavelength region, including the light spectrum where the photoactive blend absorbs. Reduced amount of reflected light can lower the J_{SC} as the 160 nm thick active layer is not sufficient to absorb most of the incoming light in one pass.[24]

To identify the origin of the increased parasitic absorption we prepared three different types of test structures either with or without photoactive layer. First samples are aimed to probe the change of the bottom cathode with glass/ITO/ZnO, and hence Ag was only deposited after aging. Another set of samples allowed us to investigate the alteration of the top anode with the following two structures: glass/MoO_3/Ag and glass/MoO_3/Ag/Al with and without the P3HT:PCBM layer. All three test structures were aged in three monostress conditions in inert atmosphere comparing the annealing at 85 °C in dark, solar illumination at 35 °C with a reference sample stored in dark at 25 °C. This systematic series of test structures allowed us to identify that the decrease in reflectance is only observed in samples with MoO_3/Ag/Al aged at elevated temperature in dark independent of the presence of the photoactive layer, as shown in Figure 3. Interestingly, the MoO_3/Ag stack aged in identical conditions maintained an elevated reflectance suggesting that Al plays a critical role in the degradation process. We also noted that the reflectance declines in the first 300 h and remains unchanged afterward, which allowed us to link this process to the evolution of the electrical performance during burn-in. Since no changes in the optical properties of the glass/ITO/ZnO stack can be observed upon aging in the different conditions, we can exclude the contribution of this electrode to the reflectivity decrease (Supporting Information, Figure S3). Similarly, solar illumination in inert condition does not alter the optical properties of

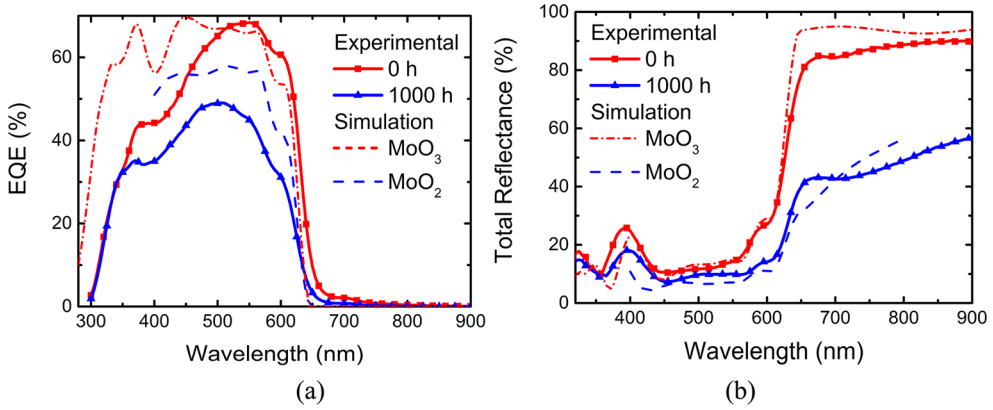

Figure 2. Spectral response (a) and total reflectance (b) measurements of devices as processed and upon 1000 h of aging under continuous illumination at 65 °C and corresponding optical simulation results (dashed lines) for device stacks either with MoO_3 or MoO_2 as transport layers.

DOI: 10.1021/am506771e
ACS Appl. Mater. Interfaces 2015, 7, 618−623

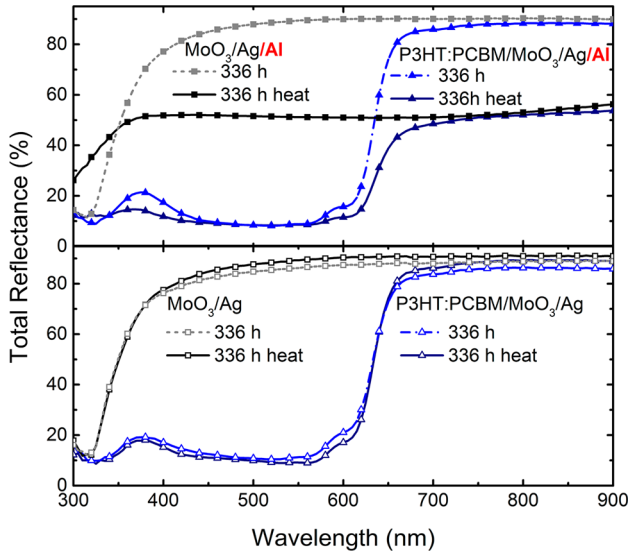

Figure 3. Reflectance measurement of test structures with Ag/Al (upper) or Ag (lower) top contacts measured upon 336 h of aging in dark and inert atmosphere either at 85 °C (full lines) or 25 °C (dashed lines). The top metal is either deposited directly on glass/MoO_3 (squares) or glass/P3HT:PCBM/MoO_3 (triangles) stacks.

the different electrode structures over 300 h. These control measurements further confirm that the presence of Al is the culprit in the reduced reflectivity signal and that the process is triggered at elevated temperature.

The reported total reflectance measurements sum the contribution of specular and diffuse components. To decouple these parts, we measured the diffuse reflectance, which only changes from 6 to 7% and to 5% above 650 nm in as-prepared and aged devices, respectively. This allows us to conclude that increased light scattering can be excluded as the origin of parasitic absorption in the top electrode and at its interfaces.

The role of Al in the reflectance loss is confirmed by conducting EDS analysis on cross sections of the entire device stack. In aged devices the Al appears to diffuse through the Ag layer (150 nm) and accumulate at the interface of the MoO_3/Ag as presented in Figure 4 (lower right). Control samples stored for the same duration at 25 °C and dark showed no Al signal above the background in the Ag or MoO_3 confirming that Al migration is triggered by elevated temperature. The presence of carbon in the MoO_3 and Ag is due to contamination during the TEM analysis. The specimens cannot be plasma-cleaned since this process etches the P3HT:PCBM layer and provokes Ag diffusion over the specimen surface.

Since Al−Ag interdiffusion could result from ion bombardment during the focused ion beam (FIB) specimen preparation, we supplemented our study with XRD of a MoO_3/Ag/Al layer stack before and after 300 h of annealing at 85 °C (Supporting Information, Figure S5). In the as-deposited MoO_3/Ag/Al sample a single peak at 38.1° is initially observed, which can be ascribed to (111) phase of textured Al. Upon annealing, this peak is replaced by three peaks at 35.9°, 39.2°, and 41.1°. These peaks correspond to the signature of the intermetallic compound of Ag_2Al (COD card 00−150−9589) confirming the intermixing of Al with Ag in aged devices.

Direct contact between MoO_3 and Al can trigger a chemical reaction between the two compounds as reported previously.[25] Chemical analysis with XPS combined with depth profiling enabled us not only to reveal Al in the Ag but also to detect its oxidation close to the MoO_3 layer. In Figure 5, we report the

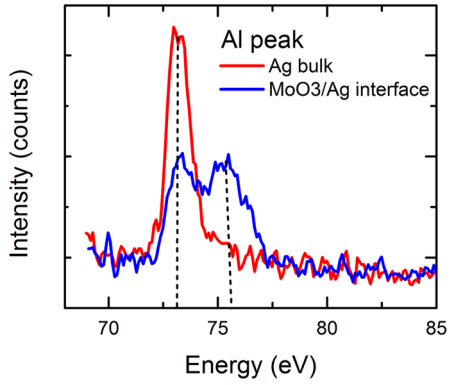

Figure 5. X-ray photoemission spectroscopy analysis of the Al 2p peak in devices upon 1000 h of aging under solar light at 85 °C either in the bulk of the Ag and at the MoO_3/Ag interface.

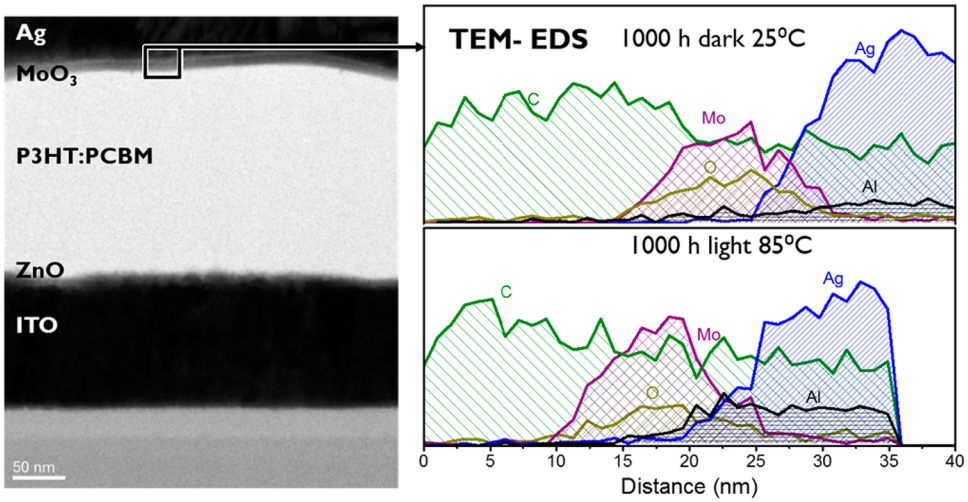

Figure 4. Transmission electron microscope cross section of an aged device (left) in bright field imaging mode and energy dispersive spectroscopy (right) at the P3HT:PCBM/MoO_3/Ag interface upon 1000 h of aging either in dark at 25 °C (upper right) or under solar light at 85 °C (lower right).

DOI: 10.1021/am506771e
ACS Appl. Mater. Interfaces 2015, 7, 618−623

signal corresponding to the Al 2p peak at two different locations in the device stack: in the bulk of the Ag layer and at the interface of MoO_3/Ag. At the former location one main peak at 73.1 eV is detected, typical of Al in its metallic state. The fact that Al in the bulk of Ag is not oxidized indicates that probably air ingress through the packaging is not the source of oxygen, which would cause a homogeneous Al oxidation in the entire layer. In contrast, at the interface of MoO_3 an additional peak at 75.3 eV is observed, suggesting oxidation of the Al. Unfortunately, the Mo 3d peaks were not reliably recorded during the sputtering to correlate the oxidation of Al directly to the reduction of MoO_3. However, this chemical reaction has been observed in thin films even in the presence of a small amount of Al and at room temperature. Furthermore, wet chemical reaction studies have also shown that MoO_3 is rapidly reduced in the presence of Al.[26]

Reduction of MoO_3 to MoO_2 among other compounds results in increased absorption in the buffer layer, leading to a significantly reduced back reflection from the top contact. To quantitatively assess the implication of this material modification, we performed optical simulation of entire device layer stack using the transfer matrix formalism. To estimate the reflectance and spectral response change upon aging, we assumed that the 10 nm thick MoO_3 layer is entirely reduced to MoO_2. The simulated reflectance of the device decreases from 90% to 50% as presented in Figure 2b, corroborating the experimental results. This reduced reflectance translates into peak spectral response decrease from 65% to 58% according to the simulation, while experimental results drop to 48%. This clear underestimation of spectral response of aged device response is probably explained by the contribution of other loss mechanisms, namely, the reorganization of the bulk heterojunction morphology and increased workfunction. A shift in the workfunction of MoO_3 from approximately −6.5 to −4.9 eV in its reduced form is expected based on previous reports.[27] As a result an energy barrier at the P3HT/$MoO_{x<3}$ interface is probably formed leading to an increase of the series resistance, which we indeed observe in our devices: from 2.8 to 19.5 Ω cm upon 1000 h of aging. These values are extracted by fitting the one diode model to the current density−voltage graphs recorded in dark (Supporting Information, Figure S6). Moreover formation of a thin insulating Al_xO_y layer at the interface can also contribute to the increase of the series resistance. Next to the change in optical properties and energy level, the conductivity of MoO_3 is also increased upon its reduction. Although an increase in shunt current is consequently expected in aged devices, this parameter remains unchanged upon aging in our devices as the MoO_3 layer is patterned (Figure S6).

In summary, we can estimate that 20% of the J_{SC} loss is linked to the change in the optical parameters of the MoO_3 layer triggered by the migration of Al, which makes this process one of the dominating failure mechanisms in this specific device.

4. CONCLUSIONS

In conclusion, we measured the performance evolution of prototypical P3HT:PCBM cells with MoO_3/Ag/Al (10:150:150 nm) anode under accelerated operational conditions. Exponential performance loss of 50% in the first 100 h, the so-called burn-in process, mainly arises from the decease of J_{SC} in our devices. Concurrently reduced reflectance above 650 nm, beyond the absorption region of the photoactive layer, hinted at a failure linked to the electrodes. Systematic aging of various test structures confirmed that the lowered reflectance arises solely in samples with Al, independent of the presence of the active layer. Decoupling the impact of solar light, heat, and storage by aging test structures in controlled environments led us to the conclusion that sample temperature of 85 °C can trigger this failure mechanism in less than 300 h. Elemental analysis of the device cross section with TEM revealed the migration of Al and its accumulation at the MoO_3/Ag interface. Both XRD and XPS corroborated this observation and further indicated a chemical reaction. In a reference stack XRD showed the formation of Ag_2Al after annealing at similar conditions, hence, confirming the Al migration. We could also reveal at interface of Ag/MoO_3 a shift in the binding energy of Al 2p peak suggesting the formation of aluminum oxide. As Al is not oxidized in the bulk of the Ag layer, we surmise that oxidation of Al occurs in contact with MoO_3; hence, this latter compound is reduced to $MoO_{x<3}$. This results inevitably in changes of the optical and electrical properties of this critical interface layer. Simulation of the optical response of the device stack with MoO_2 matched the experimental response of the aged cells providing indirect proof for the alteration of the MoO_3. Furthermore, we could estimate that 20% of the initial J_{SC} loss is linked to this failure mechanism, which makes it one of the dominating failure mechanisms in these devices.

Since this degradation process is photoactive-layer independent, insights are relevant for a variety of organic and hybrid thin-film PV cells and modules. Our understanding not only provides guidelines for material selection for stable devices but also indicates that temperature as acceleration factor is well-suited to screen for this failure mechanism.

■ ASSOCIATED CONTENT

Supporting Information

Electrical data on the reproducibility of the device stability measurements. We also report the results of Ca test, reflectivity and current density−voltage measurements, and XRD characterization of the different aged devices and layers. This material is available free of charge via the Internet at http://pubs.acs.org.

■ AUTHOR INFORMATION

Corresponding Author

*E-mail: eszter.voroshazi@imec.be.

Notes

The authors declare no competing financial interest.

■ ACKNOWLEDGMENTS

The authors like to acknowledge J. Tait for AFM measurements. The research leading to these results has received funding from the European Community's Seventh Framework Programme (FP7/2007-2013) under Grant No. 604148 of the MUJULIMA Project.

■ REFERENCES

(1) Green, M. A.; Emery, K.; Hishikawa, Y.; Warta, W.; Dunlop, E. D. Solar Cell Efficiency Tables (Version 43). *Prog. Photovoltaics* **2014**, *22*, 1−9.

(2) Peters, C. H.; Sachs-Quintana, I. T.; Kastrop, J. P.; Beaupré, S.; Leclerc, M.; McGehee, M. D. High Efficiency Polymer Solar Cells with Long Operating Lifetimes. *Adv. Energy Mater.* **2011**, *1*, 491−494.

(3) Zimmermann, B.; Würfel, U.; Niggemann, M. Longterm Stability of Efficient Inverted P3HT:PCBM Solar Cells. *Sol. Energy Mater. Sol. Cells* **2009**, *93*, 491−496.

DOI: 10.1021/am506771e
ACS Appl. Mater. Interfaces 2015, 7, 618−623

(4) Sun, Y.; Takacs, C. J.; Cowan, S. R.; Seo, J. H.; Gong, X.; Roy, A.; Heeger, A. J. Efficient, Air-Stable Bulk Heterojunction Polymer Solar Cells Using MoOx as the Anode Interfacial Layer. *Adv. Mater.* **2011**, *23*, 2226−2230.
(5) Lloyd, M. T.; Olson, D. C.; Lu, P.; Fang, E.; Moore, D. L.; White, M. S.; Reese, M. O.; Ginley, D. S.; Hsu, J. W. P. Impact of Contact Evolution on the Shelf Life of Organic Solar Cells. *J. Mater. Chem.* **2009**, *19*, 7638−7642.
(6) Lee, K.; Kim, J. Y.; Park, S. H.; Kim, S. H.; Cho, S.; Heeger, A. J. Air-Stable Polymer Electronic Devices. *Adv. Mater.* **2007**, *19*, 2445−2449.
(7) Hau, S. K.; Yip, H.-L.; Baek, N. S.; Zou, J.; O'Malley, K.; Jen, A. K.-Y. Air-Stable Inverted Flexible Polymer Solar Cells Using Zinc Oxide Nanoparticles as an Electron Selective Layer. *Appl. Phys. Lett.* **2008**, *92*, 253301.
(8) Girotto, C.; Voroshazi, E.; Cheyns, D.; Heremans, P.; Rand, B. P. Solution-Processed MoO_3 Thin Films as a Hole-Injection Layer for Organic Solar Cells. *ACS Appl. Mater. Interfaces* **2011**, *3*, 3244−3247.
(9) Zilberberg, K.; Trost, S.; Schmidt, H.; Riedl, T. Solution Processed Vanadium Pentoxide as Charge Extraction Layer for Organic Solar Cells. *Adv. Energy Mater.* **2011**, *1*, 377−381.
(10) Lloyd, M. T.; Olson, D. C.; Berry, J. J.; Kopidakis, N.; Reese, M. O.; Steirer, K. X.; Ginley, D. S. Enhanced Lifetime in Unencapsulated Organic Photovoltaics with Air Stable Electrodes. *35th IEEE Photovoltaics Specialst Conference (PVSC)* **2010**, 1060−1063.
(11) Voroshazi, E.; Cardinaletti, I.; Uytterhoeven, G.; Li, S.; Empl, M.; Aernouts, T.; Rand, B. P. Role of Electron- and Hole-Collecting Buffer Layers on the Stability of Inverted Polymer: Fullerene Photovoltaic Devices. *IEEE J. Photovoltaics* **2014**, *4*, 265−270.
(12) Khelifi, S.; Voroshazi, E.; Spoltore, D.; Piersimoni, F.; Bertho, S.; Aernouts, T.; Manca, J.; Lauwaert, J.; Vrielinck, H.; Burgelman, M. Effect of Light Induced Degradation on Electrical Transport and Charge Extraction in Polythiophene:Fullerene (P3HT:PCBM) Solar Cells. *Sol. Energy Mater. Sol. Cells* **2014**, *120*, 244−252.
(13) Voroshazi, E.; Verreet, B.; Aernouts, T.; Heremans, P. Long-Term Operational Lifetime and Degradation Analysis of P3HT:PCBM Photovoltaic Cells. *Sol. Energy Mater. Sol. Cells* **2011**, *95*, 1303−1307.
(14) Bertho, S.; Haeldermans, I.; Swinnen, A.; Vandewal, K.; Martens, T. Effect of Temperature on the Morphological and Photovoltaic Stability of Bulk Heterojunction Polymer:Fullerene Solar Cells. *Sol. Energy Mater. Sol. Cells* **2008**, *92*, 753−760.
(15) Distler, A.; Sauermann, T.; Egelhaaf, H.-J.; Rodman, S.; Waller, D.; Cheon, K.-S.; Lee, M.; Guldi, D. M. The Effect of PCBM Dimerization on the Performance of Bulk Heterojunction Solar Cells. *Adv. Energy Mater.* **2014**, *4*, 1300693−1300699.
(16) Hintz, H.; Sessler, C.; Peisert, H. Wavelength-Dependent Pathways of Poly-3-hexylthiophene Photo-Oxidation. *Chem. Mater.* **2012**, *24*, 2739−2743.
(17) Manceau, M.; Rivaton, A.; Gardette, J.-L.; Guillerez, S.; Lemaître, N. The Mechanism of Photo- and Thermooxidation of Poly(3-hexylthiophene) (P3HT) Reconsidered. *Polym. Degrad. Stab.* **2009**, *94*, 898−907.
(18) Reese, M. O.; Gevorgyan, S. a.; Jørgensen, M.; Bundgaard, E.; Kurtz, S. R.; Ginley, D. S.; Olson, D. C.; Lloyd, M. T.; Morvillo, P.; Katz, E. A.; Elschner, A.; Haillant, O.; Currier, T. R.; Shrotriya, V.; Hermenau, M.; Riede, M. R.; Kirov, K.; Trimmel, G.; Rath, T.; Inganäs, O.; Zhang, F.; Andersson, M.; Tvingstedt, K.; Lira-Cantu, M.; Laird, D.; McGuiness, C.; Gowrisanker, S.; Pannone, M.; Xiao, M.; Hauch, J.; Steim, R.; DeLongchamp, D. M.; Rösch, R.; Hoppe, H.; Espinosa, N.; Urbina, A.; Yaman-Uzunoglu, G.; Bonekamp, J.-B.; van Breemen, A. J.J.M.; Girotto, C.; Voroshazi, E.; Krebs, F. C. Consensus Stability Testing Protocols for Organic Photovoltaic Materials and Devices. *Sol. Energy Mater. Sol. Cells* **2011**, *95*, 1253−1267.
(19) White, M. S.; Olson, D. C.; Shaheen, S. E.; Kopidakis, N.; Ginley, D. S. Inverted Bulk-Heterojunction Organic Photovoltaic Device Using a Solution-Derived ZnO Underlayer. *Appl. Phys. Lett.* **2006**, *89*, 143517.
(20) Cheyns, D.; Gommans, H.; Odijk, M.; Poortmans, J.; Heremans, P. Stacked Organic Solar Cells Based on Pentacene and C_{60}. *Sol. Energy Mater. Sol. Cells* **2007**, *91*, 399−404.
(21) Schubert, S.; Klumbies, H.; Müller-Meskamp, L.; Leo, K. Electrical Calcium Test for Moisture Barrier Evaluation for Organic Devices. *Rev. Sci. Instrum.* **2011**, *82*, 09410.
(22) Klumbies, H.; Karl, M.; Hermenau, M.; Rösch, R.; Seeland, M.; Hoppe, H.; Müller-Meskamp, L.; Leo, K. Water Ingress into and Climate Dependent Lifetime of Organic Photovoltaic Cells Investigated by Calcium Corrosion Tests. *Sol. Energy Mater. Sol. Cells* **2014**, *120*, 685−693.
(23) Hermenau, M.; Schubert, S.; Klumbies, H.; Fahlteich, J.; Müller-Meskamp, L.; Leo, K.; Riede, M. The Effect of Barrier Performance on The Lifetime of Small-Molecule Organic Solar Cells. *Sol. Energy Mater. Sol. Cells* **2012**, *97*, 102−108.
(24) Dennler, G.; Scharber, M. C.; Brabec, C. J. Polymer-Fullerene Bulk-Heterojunction Solar Cells. *Adv. Mater.* **2009**, *21*, 1323−1338.
(25) Tao, C.; Ruan, S.; Zhang, X.; Xie, G.; Shen, L.; Kong, X.; Dong, W.; Liu, C.; Chen, W. Performance Improvement of Inverted Polymer Solar Cells with Different Top Electrodes by Introducing a MoO_3 Buffer Layer. *Appl. Phys. Lett.* **2008**, *93*, 193307.
(26) Schoenitz, M.; Umbrajkar, S. M. .; Dreizin, E. L. Kinetic Analysis of Thermite Reactions in Al-MoO3 Nanocomposites. *J. Propul. Power* **2007**, *23*, 683−687.
(27) Griffi, J.; Watters, D. C.; Yi, H.; Iraqi, A.; Lidzey, D.; Buckley, A. R. The Influence of MoOx Anode Stoicheometry on the Performance of Bulk Heterojunction Polymer Solar Cells. *Adv. Energy Mater.* **2013**, *7*, 903−908.

DOI: 10.1021/am506771e
ACS Appl. Mater. Interfaces 2015, 7, 618−623